High Energy Diffraction

(Invited talk, XVII International Symposium on Lepton Photon Interactions, Beijing)

Ch. Berger

I. Physikalisches Institut, RWTH-Aachen

D 52056 Aachen, Germany

E-mail: berger@rwth-aachen.de

ABSTRACT

Recent experiments on total hadronic cross sections are reviewed together with results on photo- and electroproduction of vector mesons. New data on diffractive deep inelastic scattering shed light on the nature of the pomeron.

1. Introduction

High energy scattering reactions can be roughly divided into two classes:

The first class contains the reactions involving the point-like scattering of the building blocks of the standard model via exchange of gauge bosons. The classical example is electron positron annihilation into μ pairs or quark anti-quark pairs. At high energies, where masses can be neglected, the cross section scales with $1/s$ where s is the squared center of mass energy.

The second class contains the scattering of hadrons, take $p\bar{p}$ or pp scattering as an example. The elastic cross section and the total cross section are roughly constant (or they even slightly increase at values of $s \geq 100$ GeV^2). The elastic cross section is sharply peaked in forward direction $d\sigma/dt \sim \exp Bt$ with t being the squared four momentum transfer. Both features are reminiscent of diffraction of light at a sphere of radius R with $\sigma \approx 2\pi R^2$ and $B \approx R^2/4$.

In quantum theory (Regge-phenomenology) these so called soft processes can be described by the exchange of *Regge-trajectories* $\alpha(t)$ yielding

$$\frac{d\sigma}{dt} \sim \left(\frac{s}{s_0}\right)^{2\alpha(t)-2} \tag{1}$$

where s_0 is a scale in the order of 1 GeV^2. By virtue of the optical theorem it follows for the total cross section

$$\sigma \sim \left(\frac{s}{s_0}\right)^{\alpha(0)-1} . \tag{2}$$

The *pomeron*-trajectory $\alpha_{I\!P}(0) = 1 + \epsilon$, ϵ being a small positive number, therefore leads to cross sections rising with a power law in energy.

It has been known for a long time that photons interacting with nucleons at high energies show a hadronic behavior. Photo-production can also be studied in the $Q^2 = 0$ limit of inelastic electron scattering (electro-production), where Q^2 is the negative four momentum transfer squared between in- and out- going electron.

In this context ep scattering is especially interesting, because by controlling Q^2 one can go from the hadronic (quasi real) photo-production cross section ($Q^2 \approx 0$) to the point-like deep inelastic electron proton scattering at high Q^2. The relevance of HERA with regard to this topic is due to the much higher values of Q^2 and W^2 (the squared center of mass energy of the hadronic system) reached compared with previous experiments. It is also important that in contrast to earlier fixed target experiments photo-production and deep inelastic scattering (DIS) is now studied in the same detector.

The two different worlds are even reflected in the kinematical notations. Results on photo-production are usually given in terms of photo-absorption cross sections $\sigma_{T,L}$, whereas DIS results are quoted in terms of structure functions $F_{1,2}$. For all values of Q^2 they are connected via

$$F_1 = \frac{Q^2}{4\pi^2\alpha}\frac{\sigma_T}{2x_B} \tag{3}$$

and

$$F_2 = \frac{Q^2}{4\pi^2\alpha}(\sigma_T + \sigma_L). \tag{4}$$

Here $x_B = Q^2/(Q^2 + W^2)$ is the Bjorken scaling variable and α the fine structure constant. The quantities σ_T and σ_L represent absorptive cross sections for transverse and longitudinally polarized photons. Real photons are only transversely polarized and hence σ_L vanishes with $Q^2 \to 0$. In many analyses the longitudinal contributions are neglected and therefore one works with the simple relation

$$F_2 = \frac{Q^2}{4\pi^2\alpha}\sigma_T. \tag{5}$$

Note that the formulas given above have to be multiplied by a factor $1 - x_B$ on the right hand side in order to reproduce the original definitions of Hand [1].

2. Total Cross sections

2.1. Hadrons and real photons

In their 1992 paper Donnachie and Landshoff [2] gave a very simple and economical Regge-parameterization of all hadronic total cross sections and the photo-production cross section

$$\sigma_{tot} = Xs^{\epsilon} + Ys^{-\eta} \tag{6}$$

with the universal exponents

$$\epsilon = 0.0808, \eta = 0.4525 \tag{7}$$

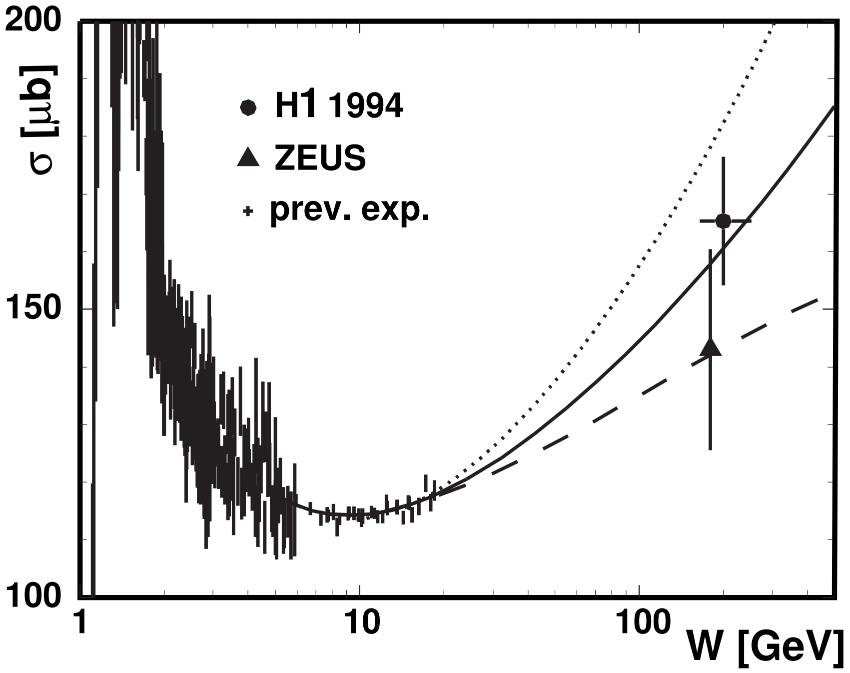

Fig. 1. Total Photo-production cross section as function of the γp center of mass energy $W_{\gamma p}$. Included are the DL [2] (full line) and ALLM [6] parameterizations (dashed line). The DL prediction is also shown for $\epsilon = 0.11$ (dotted line) as suggested by the recent CDF result [3].

The small value of ϵ results in a *soft* increase of the total cross sections at very high energies and the corresponding trajectory can therefore be named the *soft pomeron* trajectory. Note that the recent measurement $\sigma_{tot}^{p\bar{p}} = 80.03 \pm 0.93$ mb at $\sqrt{s} = 1800$ GeV by the CDF collaboration[3] lies significantly above this parameterization. Including this new value leads to $\epsilon = 0.112 \pm 0.013$ for $p\bar{p}$ scattering [3].

HERA allows the measurement of the total photo-production cross section at values of $W = \sqrt{s}$ around 200 GeV via electron tagging at 0°. The first HERA measurements [4] confirmed the soft pomeron prediction for photo-production processes. For this conference we have a new result from H1 [5] with reduced error, $\sigma_{tot}^{\gamma p} = 165 \pm 2 \pm 11$ μb, which is shown in fig. 1 together with the published ZEUS value and previous low energy data.[a] The Donnachie-Landshoff (DL) fit result [2] is represented by the full line. The two other curves represent the DL ansatz with $\epsilon = 0.11$ and a Regge-fit by Abramovicz et al. [6].

H1 provides an interesting study of the decomposition of the total γp cross section. Dividing the diffractive part of the cross section into the following classes

(quasi)-elastic	$\gamma p \to Vp$
photon dissociation	$\gamma p \to Xp$
proton dissociation	$\gamma p \to VY$
double dissociation	$\gamma p \to XY$

[a]As usual the the first error is statistical the second systematic.

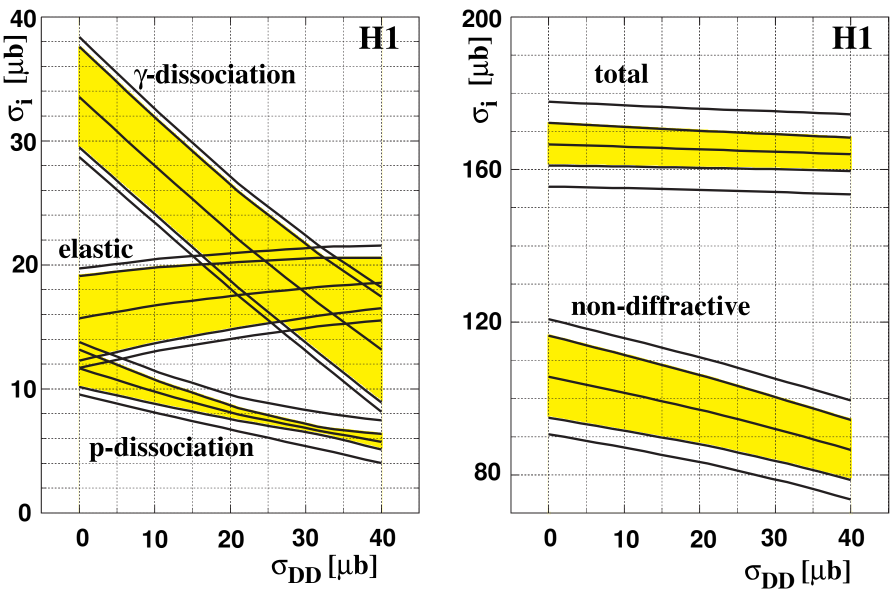

Fig. 2. The measured partial and total γp cross sections as function of the assumed double dissociative cross section. The wider bands correspond to full statistical and systematic errors added in quadrature. The narrower grey bands show the systematic error due to the model dependence described in the publication [5].

where V represents a vector meson, X another hadronic state originating from the photon-pomeron vertex and Y a hadronic state from the proton-pomeron vertex, the partial cross sections are given as function of the assumed double dissociative (DD) cross section (fig. 2). It follows that photon dissociation exceeds proton dissociation for a wide range of σ_{DD}.

2.2. Deep inelastic scattering

One of the prominent results of the HERA experiments is the strong increase of F_2 at small x_B in deep inelastic scattering experiments. This increase is very well parameterized by using the standard Altarelli-Parisi evolution equations. This good description[b] includes even the recent HERA data at Q^2 down to 2 GeV^2. At fixed Q^2 this increase at small x_B can be translated (see Eq.(4)) to an increase $\sim W^{2\epsilon}$ of $\sigma_T + \sigma_L$ at high W. The resulting values of ϵ are in the range $0.2 - 0.4$ and certainly not compatible with $\epsilon = 0.0808$. Using Regge language one can thus talk about the occurrence of a *hard* pomeron in deep inelastic scattering. Regge-models are flexible enough to deliver an interpolation between photo-production and electro-production by e.g. assuming ϵ to be Q^2 dependent [7]. Various fits to the total cross section in the whole Q^2 range have thus been achieved either based on Regge-phenomenology

[b] For more details and a discussion of the dynamical implications see the contributions of A. Caldwell and J. Bartels elsewhere in these proceedings.

alone [8] or a combination of QCD-fits with Regge-parameterizations [7].

3. Vector Meson Production

3.1. ρ photo-production

The most interesting exclusive channels to investigate in photon proton scattering are those where vector mesons are produced in the final state. For example the two body reaction $\gamma p \to \rho p$ accounts for about 10% of the total photo-production cross section. Moreover in the well known notion of vector meson dominance (VMD) these channels are intimately connected (optical theorem) to the total photo-production cross section. This field has therefore been extensively investigated in the past at center of mass energies W up to 18 GeV.

The new HERA results from the two collaborations H1 [9] and ZEUS [10] provide for the first time data at high values of W. They are shown in fig. 3 together with older low energy data. The data agree very nicely with theoretical calculations based on the additive quark model and VMD [11]. Being an exclusive channel the increase with energy is given by $W^{4\epsilon}$. The curve in fig. 3 corresponds to the DL-value $\epsilon = 0.0808$. Also the other features of the low energy data like the slope $B \approx 9$ GeV^{-2} of the t distribution and s channel helicity conservation leading to a transverse polarization of the produced ρ mesons remain valid.

3.2. ρ electro-production

Both HERA experiments ZEUS [12] and H1 [13] have extended their investigations of the reaction $ep \to e\rho p$ from $Q^2 = 0$ to 8.5 and 17 GeV^2 at high hadronic center of mass energies ($W \approx 70$ and 100 GeV). In fig. 4 the data are presented as virtual photon absorption cross sections, which to a very good approximation are given by $\sigma_T + \sigma_L$. Together with the NMC data [14] at lower energy a power law ansatz $W^{4\epsilon}$ yields $\epsilon \approx 0.20$ incompatible with the standard soft pomeron value.

The ZEUS collaboration also analyzed the slope of the t distribution and the helicity of the ρ meson. Just as for experiments at lower energy [14] they find a much shallower t distribution (B being roughly half of the photo-production value) and consistency with dominance of the longitudinal cross section σ_L.

The latter point is readily understood in perturbative quantum chromodynamics (pQCD). Helicity conservation at the photon quark vertex in fig. 5 leads to $J_z = 0$ for the total angular momentum of the quark anti-quark pair traveling along the z-axis. Therefore only longitudinally polarized photons contribute. The explicit calculation of the ρ electro-production cross section via two gluon exchange yields [15]

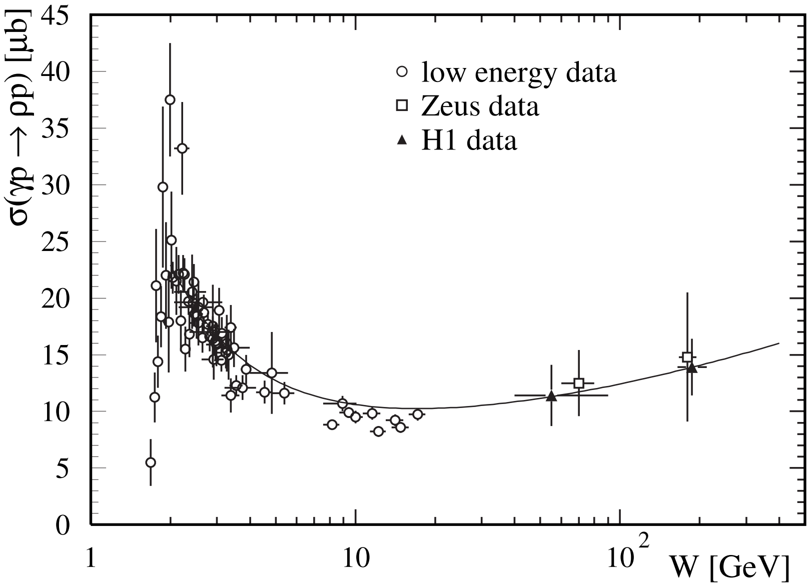

Fig. 3. Total elastic ρ photo-production ($\gamma p \to \rho p$) cross section as function of W. The HERA data [9,10] are shown together with theoretical expectations for the soft pomeron[11].

$$\left.\frac{d\sigma^{\gamma^* p}_{L,Vp}}{dt}\right|_{t=0} = \frac{\pi^3 \Gamma_V^{e^+e^-} M_V \alpha_S(Q^2) \eta_V^2 \left| xg(x,Q^2) + \imath \frac{\pi}{2} \frac{d}{d \ln x} xg(x,Q^2) \right|^2}{3 \alpha Q^6} \tag{8}$$

with $x = Q^2/W^2 \ll 1$. M_V is the mass of the produced vector meson, α_S the strong coupling constant and η_V a factor related to the vector meson wave function.

Using the measured slope in t and the measured ratio σ_L/σ_T this formula can be converted into a prediction for $\sigma(\gamma^* p \to \rho p)$. The result of the ZEUS analysis [12] is shown in fig. 6. The pQCD calculation can roughly account for the strong increase in W, which is intuitively understandable because the gluon density $g(x, Q^2)$ with its strong increase at small x enters quadratically into Eq.(8). The theoretical prediction has a large uncertainty. In addition to the errors in the measurement of the gluon density g the meaning of the arguments x and Q^2 is not really clear because the two gluons couple to quarks of different momenta. It will therefore be difficult to use these experiments for a precision determination of $g(x, Q^2)$.

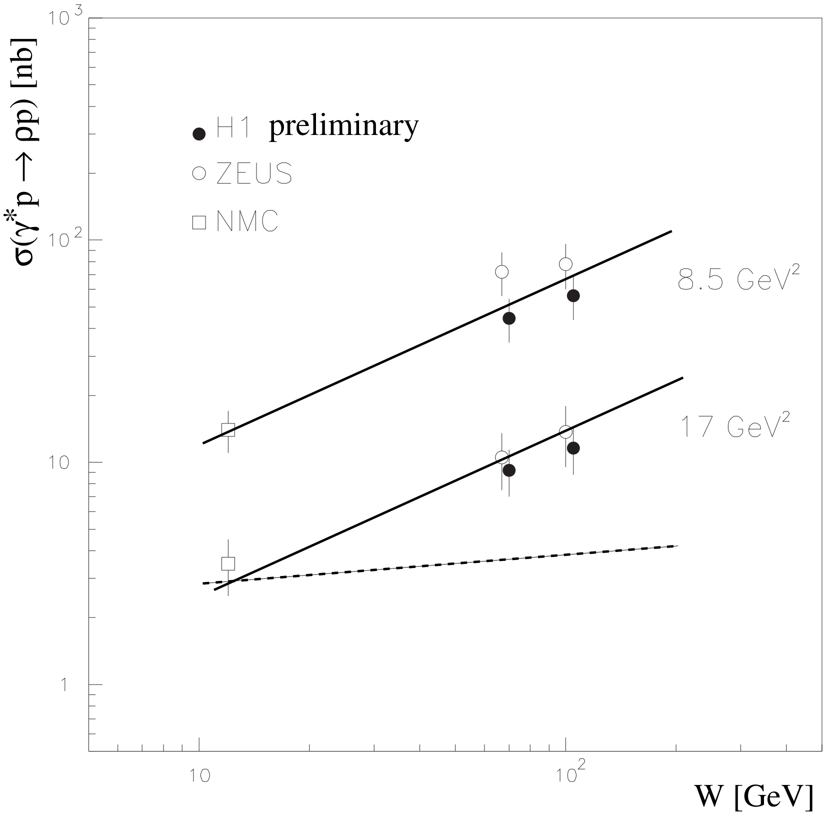

Fig. 4. Total elastic ρ electro-production ($\gamma^* p \rightarrow \rho p$) cross section as function of W. The HERA data[12,13] are shown together with the NMC data [14] at $W = 12.9$ GeV.The full line corresponds to $W^{4\epsilon}$ with $\epsilon = 0.2$, the dashed line to $\epsilon = 0.08$.

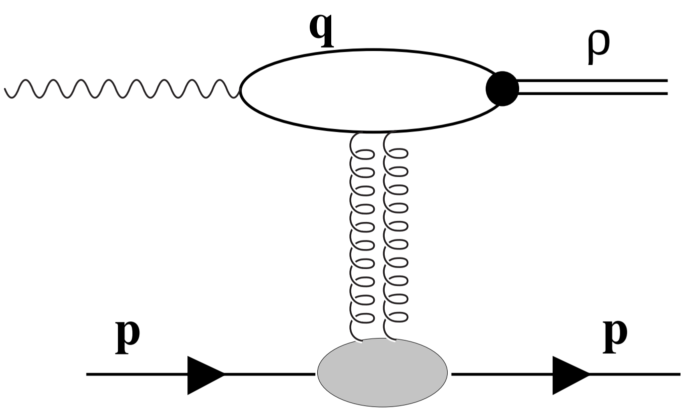

Fig. 5. ρ electro-production via two gluon exchange ($\gamma^* p \rightarrow \rho p$)

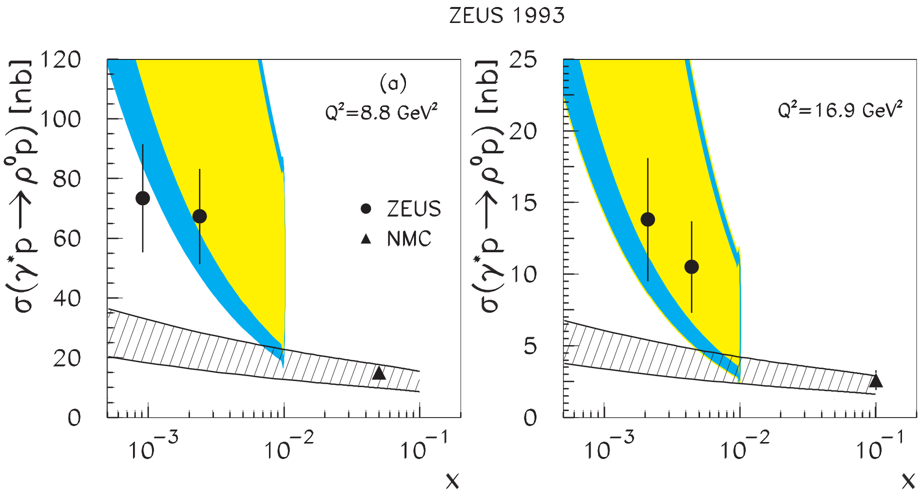

Fig. 6. High W total elastic ρ electro-production ($\gamma^* p \rightarrow \rho p$) cross section in comparison with a pQCD calculation [15]. The experimental errors shown are only statistical. The range in the light shaded area is due to the experimental uncertainty of the gluon density entering the QCD calculation. The dark shaded area includes the uncertainty on B and σ_L/σ_T. The hatched area displays the cross section expected from a soft pomeron model [16].

3.3. J/ψ photo-production and electro-production

Photo-production of J/ψ mesons is not just a repetition of the ρ meson scenario. First of all the total cross section for exclusive production of J/ψ's at $W \approx 10$ GeV is about a factor of 1000 smaller than the ρ cross section. This fact has always puzzled a straightforward interpretation in terms of vector meson dominance. Secondly results from the Fermi-lab experiment E401 [17] reaching center of mass energies around 20 GeV already indicated a stronger increase with W. The new HERA data [18,19] together with the recent results from E687 [21] confirm unambiguously this steep increase. This is demonstrated in fig. 7, where the solid line corresponds to $\epsilon = 0.0808$ in the $W^{4\epsilon}$ ansatz , whereas the dashed line is calculated with $\epsilon = 0.25$. A universal soft pomeron trajectory is therefore incompatible with the data in fig. 7, but the pQCD calculation of Ryskin [20] based again on two gluon exchange can within large uncertainties due to the gluon density parameterizations describe the experimental results.

It has been observed in previous experiments (e.g. EMC [22]) that the cross section for light and heavy vector mesons become similar with increasing values of Q^2. H1 [23] presents for the first time data on exclusive electro-production of J/ψ mesons for rather high virtual photon masses ($Q^2 = 17$ GeV^2) *and* very high hadronic center of mass energies, $W = 60$ and 80 GeV. They are shown in fig. 8 together with H1 results for photo-production of J/ψ's and photo- and electro-production of ρ mesons. The elastic J/ψ cross sections at $Q^2 = 17$ GeV^2 in fig. 8 are factor of 2 smaller than the published data [23] which still include proton dissociation. A more detailed

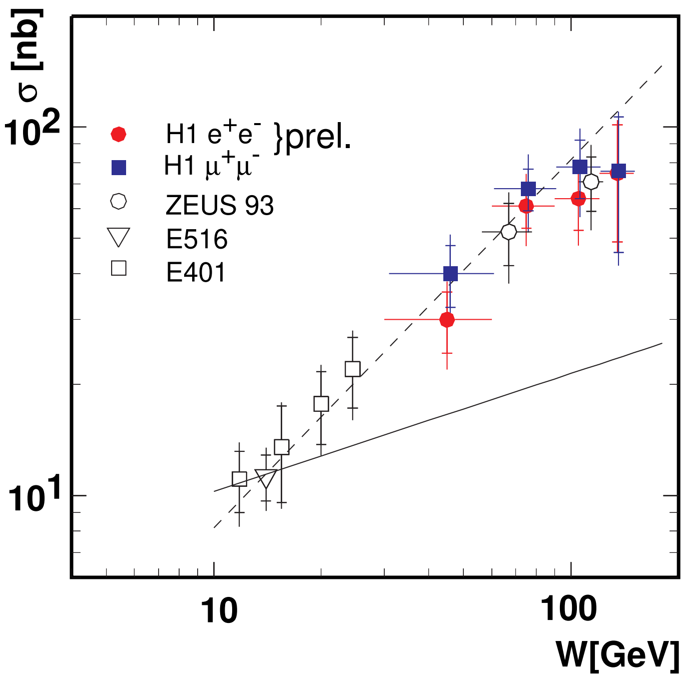

Fig. 7. The total cross section for elastic J/ψ photo-production versus the center of mass energy W. The dashed line correspond to $W^{4\epsilon}$ with $\epsilon = 0.25$ whereas the full line belongs to $\epsilon = 0.0808$.

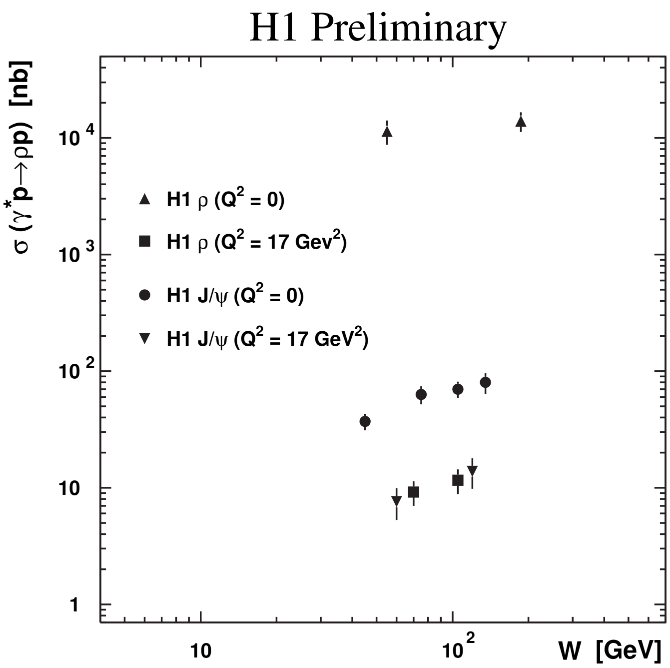

Fig. 8. Recent H1 data [23] for elastic photo-production and electro-production of vector mesons versus the hadronic center of mass energy W.

determination of this correction factor is under study.

As can be seen from the figure the increase in W is compatible with the increase found for J/ψ production at $Q^2=0$ and for ρ production at $Q^2 = 17$ GeV^2. There seems to be a sharp increase of the ϵ coefficient ($\epsilon \geq 0.20$) whenever a high mass scale (M_V or Q^2) comes into the game. Most strikingly the cross sections for ρ and J/ψ electro-production are practically equal, indicating that at these values of Q^2 they are mainly determined by $\alpha_s(Q^2)\Gamma^V_{e^+e^-}g^2(Q^2/W^2,Q^2)$ (see Eq.(8)).

4. Diffraction in deep inelastic scattering

4.1. Basics

It is very tempting to view the pomeron as an object, whose structure can be tested in deep inelastic scattering reactions, $e\mathbb{P} \rightarrow eX$. This view has been pioneered by Ingelman and Schlein [24]. Neglecting longitudinal contributions the cross section formula can be written in close analogy to deep inelastic electron nucleon scattering as

$$\frac{d\sigma}{d\beta dQ^2} = \frac{4\pi\alpha^2}{Q^4\beta}(1-y+y^2/2)F_2^{\mathbb{P}}(\beta,Q^2) \tag{9}$$

where y is the relative energy loss of the electron in the proton rest-frame and β plays the role of x_B in electron proton scattering, i.e.

$$\beta = \frac{Q^2}{2q\cdot p_{\mathbb{P}}} = \frac{Q^2}{Q^2+M_X^2}. \tag{10}$$

In the quark model β is identified with the fractional momentum of the quarks inside the pomeron, $\beta = z_{q/\mathbb{P}}$.

Assuming that a pomeron with momentum fraction $x_{\mathbb{P}}$

$$x_{\mathbb{P}} = \frac{q\cdot P_{\mathbb{P}}}{q\cdot P} = \frac{Q^2+M_X^2}{Q^2+W^2} \tag{11}$$

of the proton momentum is radiated off the proton one immediately arrives at the threefold differential cross section

$$\frac{d\sigma}{d\beta dQ^2 dx_{\mathbb{P}}} = \frac{4\pi\alpha^2}{Q^4\beta}(1-y+y^2/2)f_{\mathbb{P}/p}(x_{\mathbb{P}})F_2^{\mathbb{P}}(\beta,Q^2). \tag{12}$$

The product of the pomeron flux factor $f_{\mathbb{P}/p}$ and the pomeron structure function $F_2^{\mathbb{P}}$ is called the threefold diffractive structure function $F_2^{D(3)}$. Note that $\beta = x_B/x_{\mathbb{P}}$ as it should be intuitively.

Eq.(12) has several important consequences, which can be tested experimentally. They are discussed in the next three subsections.

4.2. Rapidity gap events

The pomeron is a colorless object which is radiated *before* the hard scattering process. Because of the missing color interactions the signature of these events is given by large rapidity gaps in forward (proton) direction. This means that the most forward hadrons from these reactions as seen in the central detectors of ZEUS and H1 show up at rather small pseudo-rapidities[c] $\eta = -\ln\tan\theta/2$ (say $\eta_{max} \approx 2$).

This was in fact the way this class of events has been discovered [25]. For this type of selection a good instrumentation in forward direction is of vital importance [26]. Bjorken emphasizes [27] that

> *A diffractive process occurs if and only if there is a large rapidity gap in the produced-particle phase space which is not exponentially suppressed.*

Because $\ln M_X^2$ is connected with the gap $\Delta\eta$ in pseudo-rapidity [28] via $\Delta\eta \sim \ln 1/M_X^2$, one can use a plot of all DIS events versus $\ln M_X^2$ for the selection of the diffractive events. This has been done by the ZEUS collaboration [29] in a paper submitted to this conference. In fig. 9 the result is shown for $Q^2 = 14$ GeV^2 and three different bins in W. The exponential fall-off of standard DIS events and the much shallower M_X^2 dependence at small missing masses is clearly seen.

4.3. Factorization

The next important consequence of Eq.(12) is factorization, i.e. the fact that $F_2^{D(3)}$ has for all values Q^2 and β the same dependence on $x_{\mathbb{P}}$. This is indeed the case as can be seen from fig. 10, where results from H1 [26] and ZEUS [30] are combined. At fixed values of β and Q^2 the $x_{\mathbb{P}}$ dependence is related to the W^2 dependence and therefore diffraction leads to a power-law

$$\frac{d\sigma}{dx_{\mathbb{P}}\, dt} \sim x_{\mathbb{P}}^{-n} \tag{13}$$

with $n = 2\alpha(t) - 1$, as can be inferred from Eq.(1). *Assuming* an effective $t \approx 0$ between in and outgoing proton yields $n = 1 + 2\epsilon$. The H1 measurement of n results in [26] $\epsilon = 0.095 \pm 0.03 \pm 0.035$, whereas the ZEUS paper [30] has a somewhat higher value of n, giving $\epsilon = 0.15 \pm 0.04^{+0.04}_{-0.07}$. The universal power-law dependence established a clear proof of the diffractive nature of the DIS rapidity gap events [26]. Moreover both experimental results agree within errors and are compatible with the radiation of a soft pomeron.

[c]The incoming proton defines the $\theta = 0°$ axis.

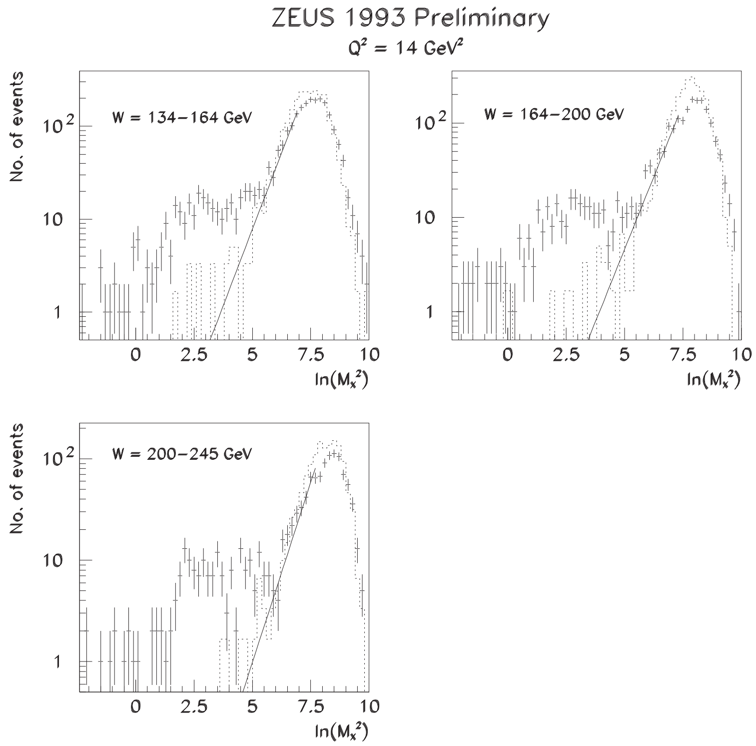

Fig. 9. Plot of all DIS events versus $\ln M_X^2$ in the ZEUS detector [29]. Diffractive events are *not* exponentially suppressed.

The new preliminary ZEUS result [29] however changes probably the last statement. The novel selection of diffractive events results in a wider range of M_X^2 and thus β compared to their previous publication [30]. A higher exponent n is found yielding $\epsilon = 0.24 \pm 0.015^{+0.07}_{-0.05}$. Although still compatible with the earlier ZEUS value and within 2σ with the H1-result, this value of ϵ lies 3σ above the standard soft pomeron ($\epsilon = 0.0808$). The analysis of the 1994 and 1995 data will hopefully show, if the factorization holds in a wide range of Q^2 and β and if a precise universal value of n can be derived. It should also be kept in mind that a measurement of the t dependence of the cross section might alter the connection between ϵ and n substantially [33], if $\alpha(t)$ has a significant t dependence.

4.4. The pomeron structure function $F_2^{I\!P}$

Because the absolute normalization of the pomeron flux factor $f_{I\!P/p}$ is not known, the pomeron structure function $F_2^{I\!P}(\beta, Q^2)$ is not directly accessible experimentally. Instead an integrated structure function

$$\tilde{F}_2^D = \int_{x_{I\!P\,L}}^{x_{I\!P\,H}} F_2^{D(3)}(\beta, Q^2, x_{I\!P})\,dx_{I\!P} \tag{14}$$

has been defined [26] with fixed lower and upper integration limits $x_{I\!P\,L} = 3 \times 10^{-4}$ and

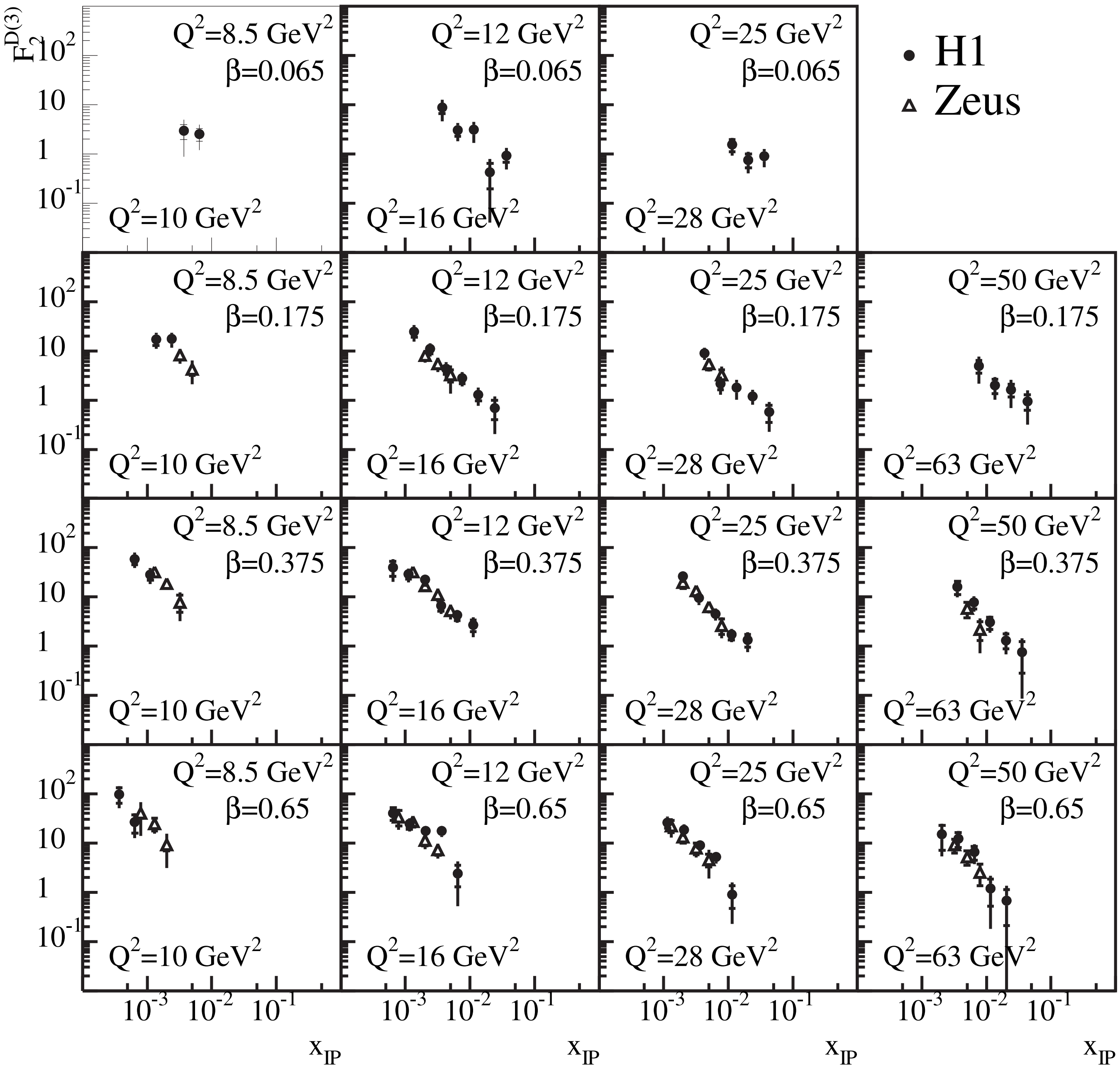

Fig. 10. $F_2^{D(3)}$ plotted versus $x_{I\!P}$ for various values of Q^2 and β. The H1-data [26] and the ZEUS-data [30] agree within errors and are compatible with an universal power law dependence on $x_{I\!P}$.

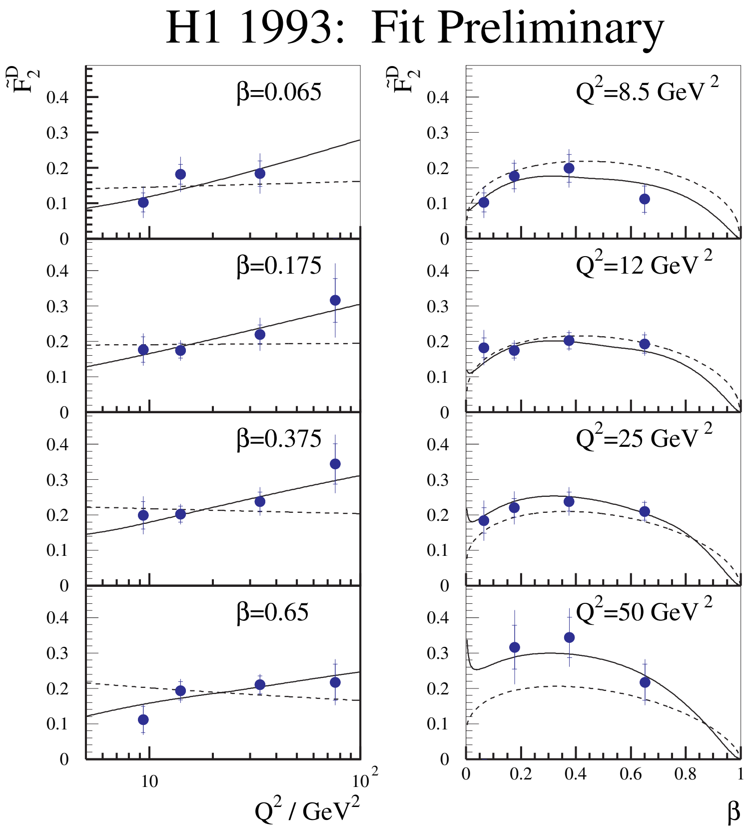

Fig. 11. Dependence of $\tilde{F}_2^D$ on Q^2 and β as seen in the H1-experiment [26]. Superimposed are fit results with quark and gluons contributing at a starting scale Q_0^2 (solid line) or with quarks only (dashed line).

$x_{\mathbb{P}\,H} = 0.05$. Assuming factorization an extension of the $x_{\mathbb{P}}$ range over the measured range in each Q^2, β bin (see fig. 10) is allowed and the resulting $\tilde{F}_2^D$ will have the same Q^2 and β dependence as the pomeron structure function.

As an example the H1 result [31] is shown in fig. 11. For all values of Q^2 the β dependence is rather flat and the Q^2 dependence at fixed β is constant or even slightly increasing. Both features are not typical for a hadronic structure function but are rather reminiscent of the Q^2 and β dependence of the photon structure function [34] F_2^γ.

More quantitatively the measured $\tilde{F}_2^D$ has been compared to models of the pomeron structure function, where in the LO-picture the electron scatters off a (anti)quark $(\bar{q})q$ in the pomeron with either a hard (e.g. $1 - z_{q/\mathbb{P}}$) or a soft quark density distribution [26,30]. The H1 collaboration now takes a step further [31] and performs a leading order (LO) Altarelli-Parisi evolution of quark and gluon densities. The solid line in fig. 11 is the result of the best fit, which started from quark and gluon input densities $q(z_{q/\mathbb{P}})$ and $g(z_{g/\mathbb{P}})$ at $Q_0^2 = 4$ GeV^2 shown in fig. 12. Taken at face value these results indicate that at the starting scale 90% of the pomeron momentum is carried by

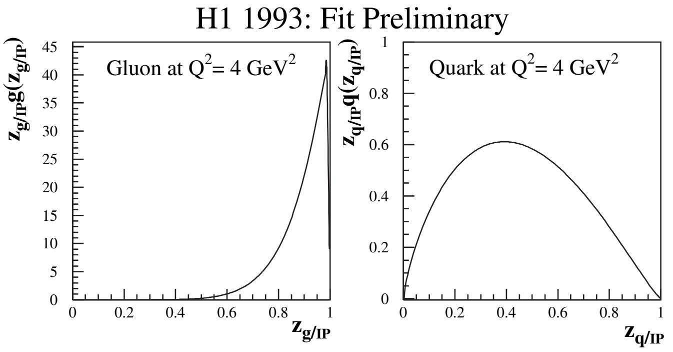

Fig. 12. The gluon density $z_{g/\mathbb{P}}\, g(z_{g/\mathbb{P}})$ and the quark flavor-singlet density $z_{q/\mathbb{P}}\, q(z_{q/\mathbb{P}})$ at a starting scale $Q_0^2 = 4$ GeV^2 belonging to the solid line in fig. 11.

gluons with a distribution very sharply peaked towards $z_{g/\mathbb{P}} = 1$. Note however that due to limited statistics the fit result is yet not very stable and a more conventional ansatz where both quark and gluon densities are $\sim 1 - z$ also leads to an acceptable fit. Even a starting distribution with quarks only is still compatible with the data (dashed line in fig. 11) at 37% C.L.

Because of the apparently gluonic nature of the pomeron diffractive scattering can be used to tag gluon initiated processes. This idea has been exploited in the calculation of diffractive Higgs production at large hadron collider (LHC) energies [35]. Fig. 13 shows the result. Although the cross section for diffractive production is naturally smaller than the total cross section for Higgs boson production, the background is probably less severe. The best fit H1 parton densities from deep inelastic electron pomeron scattering [31] and the ZEUS fit result to jet production in diffractive photoproduction [32] (see section 5) have been taken as input to the calculations. The large spread in the predicted cross section underlines that more precise experimental data are required.

4.5. A novel explanation of rapidity gap events

Rapidity gap events are all concentrated at small x_B, where the structure function F_2^p is known to be gluon driven. In a very interesting paper [36] Buchmüller and Hebecker developed an alternative explanation of the rapidity gap events. In their interpretation these events are nothing else but normal photon gluon fusion events, where the neutral cluster is formed *after* the hard scattering reaction $\gamma g \rightarrow q\bar{q}$. The neutral cluster travels without color interactions through the proton and therefore rapidity gap events occur. The detailed mechanism of the neutral cluster formation via multiple interactions with very soft partons (*wee*-partons[37]) is not yet really clear. For the time being the authors make the simple ansatz, that these clusters are just formed according to the statistical weight, i.e. in 1/9 of all low x_B photon gluon fusion events. In another context an explicit Monte Carlo model for the rearrangement of

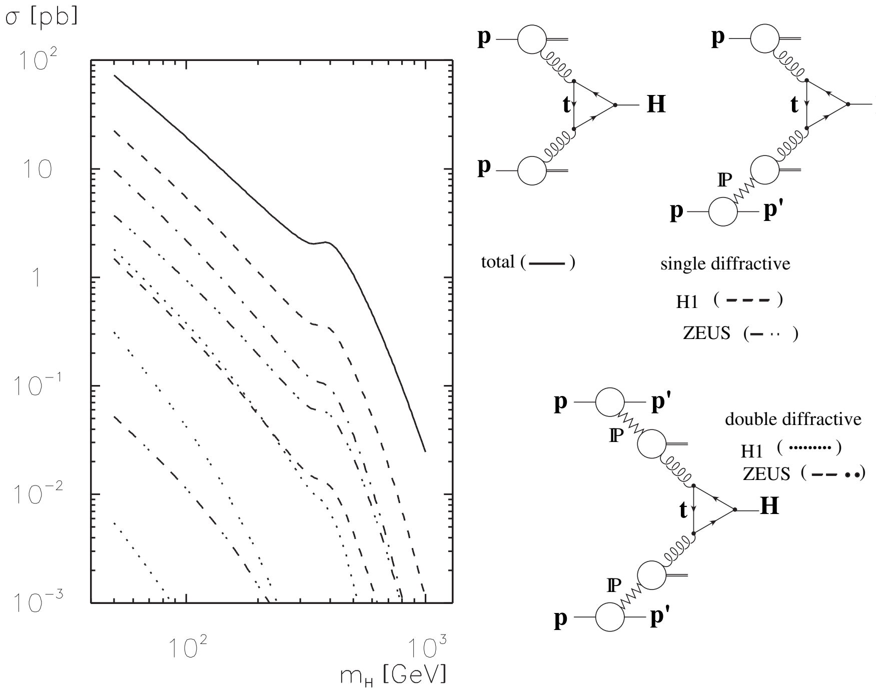

Fig. 13. Cross section for Higgs boson production [35] at LHC energies using various parameterizations of pomeron parton densities [31,32].

color has also been developed [38].

Quantitatively the calculation is carried out in the massive gluon scheme. For the proton structure function F_2 at small x_B the result

$$F_2(x_B, Q^2) \simeq \frac{\alpha_S}{3\pi} \sum_q e_q^2 x_B g(x_B) \left(\frac{2}{3} + \ln \frac{Q^2}{m_g^2} \right) \tag{15}$$

is obtained, where m_g is the virtual gluon mass. For $F_2^{D(3)}$ the approximate relation

$$F_2^{D(3)}(\beta, Q^2, z_{g/p}) \simeq \frac{1}{9} \frac{\alpha_S}{2\pi} \sum_q e_q^2 g(z_{g/p}) F_2^g(\beta, Q^2) \tag{16}$$

holds. Because the particle entering the hard scattering process is now a gluon instead of the pomeron, $x_{\mathbb{P}} = z_{\mathbb{P}/p}$ is replaced by the fractional gluon momentum $z_{g/p}$. The factor 1/9 is the statistical weight factor mentioned above and F_2^g is the structure function of the gluon. It can be calculated from the $g \to q\bar{q}$ splitting and therefore the result is very similar to the anomalous part of the photon structure function [39]:

$$F_2^g(\beta, Q^2) = \beta \left((\beta^2 + (1-\beta)^2) \ln \frac{Q^2}{m_g^2 \beta^2} - 2 + 6\beta(1-\beta) \right). \tag{17}$$

This explains immediately in a qualitative way the shallow β dependence of $\tilde{F}_2^D$ for the β values measured so far and the fact that the data show a slight increase with

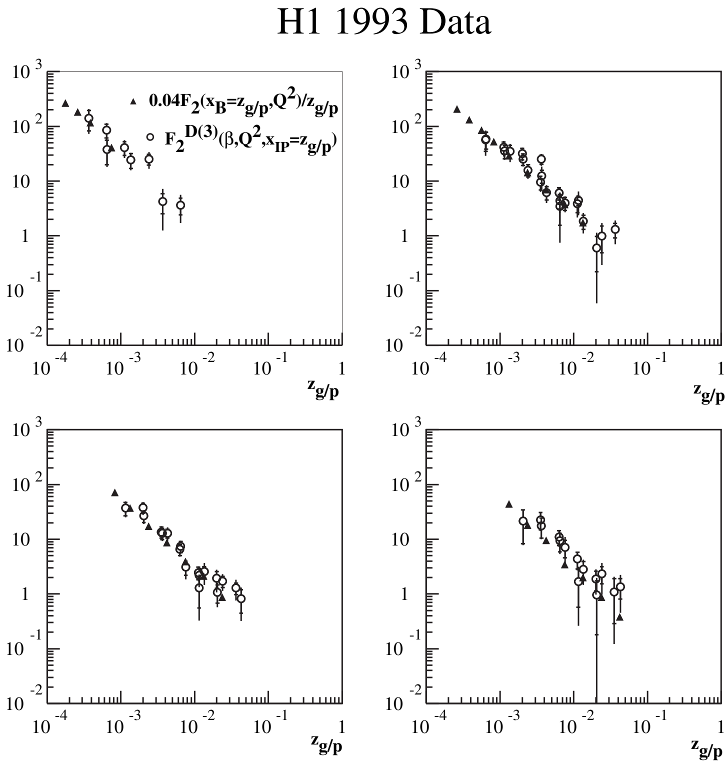

Fig. 14. Test of the scaling law Eq.(19) using H1 data [31,40].

Q^2. A detailed comparison requires probably a NLO calculation including the Q^2 dependence of α_S.

The ratio of the diffractive to the inclusive cross section can be easily calculated,

$$r_D = \frac{\int_{x_B}^{0.05} F_2^{D(3)}(x_B, Q^2, z_{g/p}) dz_{g/p}}{F_2(x_B, Q^2)} \simeq \frac{1}{9} \tag{18}$$

i.e. it is mainly given by the statistical weight factor in nice accordance with the data [30,31]. Moreover using the fact that F_2^g is approximately constant for $0.2 \leq \beta \leq 0.6$ a simple scaling law can be derived

$$F_2^{D(3)}(\beta, Q^2, z_{g/p}) \simeq \frac{0.04}{z_{g/p}} F_2(z_{g/p}, Q^2). \tag{19}$$

This certainly nontrivial prediction is tested in fig. 14 using the H1 data [31]. The different β bins for fixed values of Q^2 of fig. 10 are combined and compared with H1 structure function data [40]. The good agreement is very encouraging to follow this alternative interpretation of the rapidity gap events further.

5. Jets in diffractive final states

Further insight into the nature of diffractive scattering can be obtained by an

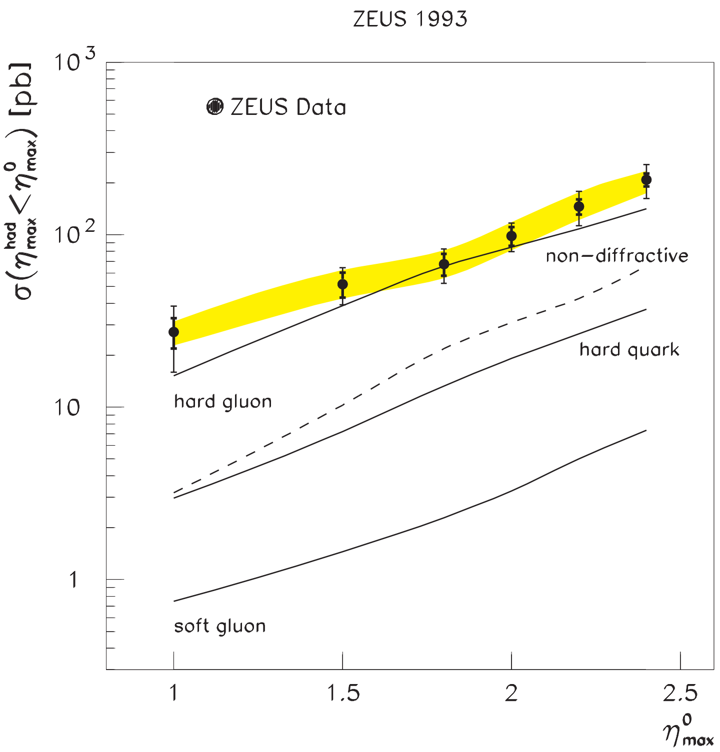

Fig. 15. The integrated inclusive jet cross section in diffractive photo-production [44] as function of the maximum pseudo-rapidity of the observed hadrons. The inner error bars are statistical only the outer error bars contain also the quadratic addition of those systematic errors which are not associated with the uncertainty in the jet energy scale. This additional error is indicated by the shaded band.

investigation of the final state. The occurrence of hard scattering in diffractive photo-production has been observed by the H1 [41] and the ZEUS [42] collaboration. In a paper contributed to this conference [43] the D0 collaboration reports on a class of events which can be interpreted as pomeron exchange between two high transverse energy jets.

In a recent publication [44] the ZEUS collaboration uses the measurement of the jet cross section in diffractive photo-production for a determination of the gluon density in the pomeron. Compared to the study of scaling violations in deep inelastic electron pomeron scattering this method allows a more direct access to the gluon density. Jets are defined using a cone algorithm with a cone radius of one unit. The measured inclusive jet cross section is compared to detailed Monte Carlo models which include the pomeron flux, the hard scattering cross sections and various models of parton densities inside the pomeron. In evaluating the theoretical prediction the ZEUS collaboration assumes the DL flux normalization [45]. The result for the integrated inclusive jet cross section as function of the maximum pseudo-rapidity of the observed hadrons is shown in fig. 15.

The inner error bars are statistical only the outer error bars contain also the

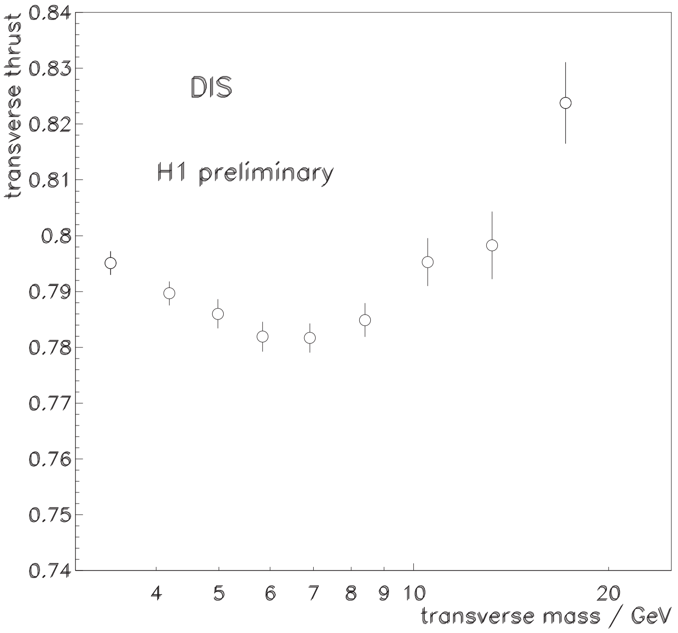

Fig. 16. Transverse thrust versus transverse mass in deep inelastic diffractive scattering. The data are not corrected for the effects of finite acceptance or resolution. Only statistical errors are shown.

quadratic addition of those systematic errors which are not associated with the uncertainty in the jet energy scale. This additional error is indicated by the shaded band. The best description of the data is obtained by the solid line labeled *hard gluon*. Here the pomeron is assumed to consist only of gluons with a density function $f_{g/\mathbb{P}} = 6(1 - z_{g/\mathbb{P}})$ neglecting the scale dependence. Other models, including non diffractive models of jet production are clearly disfavored.

Jet production in deep inelastic diffractive scattering has also been studied [46]. A model independent proof of the hard scattering structure is obtained by a study of the event topology in a plane transverse to the proton axis in the $\gamma \mathbb{P}$ center of mass frame. The event momentum vectors are projected onto this plane. From these momenta $\boldsymbol{p_T}$ the transverse invariant mass M_T and the transverse thrust $T_\perp = max(\sum \boldsymbol{p_T n} / \sum |\boldsymbol{p_T}|)$ are calculated. For spherical events $T_\perp$ reaches the limit $2/\pi$.

In fig. 16 $T_\perp$ is plotted versus M_T. The data are not corrected for the effects of finite acceptance or resolution. For small transverse masses and low hadron multiplicities statistical fluctuations may result in high values of $T_\perp$ which should decrease towards higher values of transverse masses as seen in the figure. The steep increase of the transverse thrust above $M_T \sim 8$ GeV is a clear indication that the events are now "back to back" in the transverse plane, i.e. jets are produced. Consequently jet rates and and jet properties in deep inelastic diffractive scattering have been studied [46]. Further detailed investigations will hopefully allow to discriminate between the standard picture of diffractive events and the model discussed in section 4.4.

6. Conclusions

The last two years have provided us with many exciting new results in diffractive physics. We have new results on total cross sections in $p\bar{p}$ scattering and photo-production. The new data on vector meson production are accompanied by a deeper theoretical understanding of these processes. Most importantly diffractive phenomena have been investigated in some detail in deep inelastic scattering reactions and in jet production.

I want to thank the organizers of the conference for a very interesting and well organized meeting. The help of many colleagues of the H1 and ZEUS collaboration in preparing this contribution is gratefully acknowledged.

1. L. Hand, *Phys. Rev.* **129** (1963) 1834.
2. A. Donnachie and P.V. Landshoff, *Phys. Lett.* **B296** (1992) 227.
3. CDF Collab., F. Abe et al., *Phys. Rev.* **D50** (1994) 5550.
4. H1 Collab., T. Ahmed et al., *Phys. Lett.* **B299** (1993) 374,
   ZEUS Collab., M. Derrick et al., *Z.Phys.* **C63** (1994) 391.
5. H1 Collab., S. Aid et al., *preprint DESY* **95-162** (1995).
6. H. Abramovicz, E.M. Levin, A. Levy and U. Maor, *Phys. Lett.* **B269** (1991) 465.
7. A. Kaidalov, Proceedings of the VI conference on elastic scattering and diffraction, Blois, (June 1995), ed. J. Tran Thanh Van.
8. A. Donnachie and P.V. Landshoff, *Z. Phys* **C61** (1995) 139,
   A. Levy *preprint DESY* **95-003** (1995).
9. H1 Collab., S. Aid et al., paper EPS-0473 contributed to the Int. Europhys. Conf. on HEP, Brussels, July 1995.
10. ZEUS Collab., M. Derrick et al., paper EPS-0389 contributed to the Int. Europhys. Conf. on HEP, Brussels, July 1995.
11. G.A. Schuler and T. Sjöstrand, *Nucl. Phys.* **B407** (1993) 539.
12. ZEUS Collab., M. Derrick et al., paper EPS-0397 contributed to the Int. Europhys. Conf. on HEP, Brussels, July 1995.
13. H1 Collab., paper EPS-0490 contributed to the Int. Europhys. Conf. on HEP, Brussels, July 1995.
14. NMC Collab., M. Arneado et al., *Nucl. Phys.* **B429** (1994) 503.
15. S.J. Brodsky, L. Frankfurt, J.F. Gunion and M. Strikman, *Phys. Rev.* **D50** (1994) 3134.
16. A. Donnachie and P.V. Landshoff, *Phys. Lett.* **B185** (1987) 403.
17. E401 Collab., M. Binkley et al., *Phys. Rev. Lett.* **48** (1982) 73.
18. H1 Collab., paper EPS-0468 contributed to the Int. Europhys. Conf. on HEP,

Brussels, July 1995.
19. ZEUS Collaboration M. Derrick et al., *Phys. Lett.* **B350** (1995) 120 and paper EPS-0386 contributed to the Int. Europhys. Conf. on HEP, Brussels, July 1995.
20. M. Ryskin, *Z. Phys.* **C57** (1993) 89.
21. P.L. Frabetti et al., paper contributed to the Int. Europhys. Conf. on HEP, Brussels, July 1995.
22. European Muon Collab., J. Ashman et al., *Z. Phys.* **C39** (1988) 169.
23. H1 Collab., paper EPS-0469 contributed to the Int. Europhys. Conf. on HEP, Brussels, July 1995.
24. G. Ingelman and P. Schlein, *Phys. Lett.* **B152** (1985) 256.
25. ZEUS Collab., M. Derrick et al., *Phys. Lett.* **B315** (1993) 481.
26. H1 Collab., T. Ahmed et al., *Phys. Lett.* **B348** (1995) 681.
27. J.D. Bjorken, *SLAC Pub* **6447** (1994).
28. A.B. Kaidalov, *Phys. Rep.* **50** (1979) 157.
29. ZEUS Collab., M. Derrick et al., paper contributed to the XVII International Symposium on Lepton-Photon Interactions, Beijing, (August 1995).
30. ZEUS Collab., M. Derrick et al., *preprint DESY* **95-093** (1995)
31. H1 Collab., paper EPS-0491 contributed to the Int. Europhys. Conf. on HEP, Brussels, July 1995 and H1 Collab., T. Ahmed et al., *Phys. Lett.* **B348** (1995) 681.
32. ZEUS Collab., M. Derrick et al., *preprint DESY* **95-115** (1995).
33. T. Gehrmann and W.J. Stirling, *Durham preprint* **DTP/95/26** (1995).
34. Ch. Berger and W. Wagner, *Phys. Rep.* **146** (1987) 1.
35. D. Graudenz and G. Veneziano, *preprint CERN-TH* **95-232** (1995).
36. W. Buchmüller and A. Hebecker, *Phys. Lett.* **B355** (1995) 573.
37. W. Buchmüller, *Phys. Lett.* **B353** (1995) 335 and *Phys. Lett.* **B335** (1994) 479.
38. A. Edin, G. Ingelman and J. Rathsman, *preprint DESY* **95-163** (1995).
39. T. Walsh and P. Zerwas, *Phys. Lett.* **B44** (1973) 195.
40. H1 Collab., T. Ahmed et al., *Nucl. Phys.* **B439** (1995) 471.
41. H1 Collab., T. Ahmed et al., *Nucl. Phys.* **B435** (1995) 3.
42. ZEUS Collab., M. Derrick et al., *Phys. Lett* **B346** (1995) 399.
43. D0 Collab., S. Abachi et al., paper contributed to the XVII International Symposium on Lepton-Photon Interactions, Beijing, (August 1995).
44. ZEUS Collab., M. Derrick et al., paper EPS-0378 contributed to the Int. Europhys. Conf. on HEP, Brussels, July 1995.
45. A. Donnachie and P.V. Landshoff, *Nucl. Phys.* **B303** (1988) 634 and *Phys. Lett.* **B285** (1992) 172.
46. H1 Collab., paper EPS-0494 contributed to the Int. Europhys. Conf. on HEP, Brussels, July 1995.